Acta Oceanol. Sin., 2020, Vol. 39, No. 11, P. 13–20
https://doi.org/10.1007/s13131-020-1621-1
http://www.hyxb.org.cn
E-mail: hyxbe@263.net

Influence of two inlets of the Luzon overflow on the deep circulation in the northern South China Sea

Muping Zhou[1, 2, 3], Changlin Chen[2, 4*], Yunwei Yan[3, 4], Wenhu Liu[2]

[1] College of Ocean and Earth Science, Xiamen University, Xiamen 361102, China

[2] Department of Atmospheric and Oceanic Sciences & Institute of Atmospheric Sciences, Fudan University, Shanghai 200438, China

[3] State Key Laboratory of Satellite Ocean Environment Dynamics, Second Institute of Oceanography, Ministry of Natural Resources, Hangzhou 310012, China

[4] Southern Marine Science and Engineering Guangdong Laboratory (Zhuhai), Zhuhai 519000, China

Received 21 January 2020; accepted 2 April 2020

Abstract

An inverse reduced-gravity model is used to simulate the deep South China Sea (SCS) circulation. A set of experiments are conducted using this model to study the influence of the Luzon overflow through the two inlets on the deep circulation in the northern SCS. Model results suggest that the relative contribution of these inlets largely depends on the magnitude of the input transport of the overflow, but the northern inlet is more efficient than the southern inlet in driving the deep circulation in the northern SCS. When all of the Luzon overflow occurs through the northern inlet the deep circulation in the northern SCS is enhanced. Conversely, when all of the Luzon overflow occurs through the southern inlet the circulation in the northern SCS is weakened. A Lagrangian trajectory model is also developed and applied to these cases. The Lagrangian results indicate that the location of the Luzon overflow likely has impacts upon the sediment transport into the northern SCS.

Key words: inlets, Luzon overflow, deep circulation, northern South China Sea

Citation: Zhou Muping, Chen Changlin, Yan Yunwei, Liu Wenhu. 2020. Influence of two inlets of the Luzon overflow on the deep circulation in the northern South China Sea. Acta Oceanologica Sinica, 39(11): 13–20, doi: 10.1007/s13131-020-1621-1

1 Introduction

The South China Sea (SCS) is the largest semi-enclosed marginal sea in the northwestern Pacific, bounded by the Luzon Island to the east, Kalimantan Island to the south, Vietnam to the west, and China to the north (Fig. 1a). The deepest water is confined within a bowl-shaped trench with a maximum depth of around 5 560 m (Wyrtki, 1961). The Luzon Strait is the only deep channel connecting the deep SCS water with the open ocean (Qu et al., 2006; Tian and Qu, 2012). Because the Luzon Strait has a sill depth of around 2 400 m, the deep SCS basin is completely isolated below 2 400 m.

The deep circulation in the SCS is characterized by a cyclonic gyre with a strong deep western boundary current (DWBC, Fig. 1a). This deep SCS circulation pattern and the DWBC were reported by Qu et al. (2006) from World Ocean Database and Wang et al. (2011) from the U.S. Navy Generalized Digital Environment Model (GDEM) data, the existence of DWBC was further verified by Zhou et al. (2017) from *in-situ* mooring observations, and to some extent captured by numerical simulations (Lan et al., 2013, 2015; Wang et al., 2018).

The deep circulation in the SCS results from the interaction between multi-scale dynamic processes and the complex topography (Qu, 2002; Qu et al., 2006; Tian et al., 2006; Tian et al., 2009; Chang et al., 2010; Wang et al., 2011; Lan et al., 2013; Zhao et al., 2014; Lan et al., 2015; Shu et al., 2016; Wang et al., 2016, 2018, 2019; Yang et al., 2016). Many studies have suggested that the Luzon overflow, which is comprised of the relatively cold and high-density Pacific Ocean water sinks to the SCS after it crosses the Luzon Strait, is one of the most important factors in determining the deep circulation in the SCS (Wyrtki, 1961; Qu et al., 2006; Li and Qu, 2006; Wang et al., 2011; Lan et al., 2013; Zhao et al., 2014). Based on all available hydrographic data from the World Ocean Database 2001, Qu et al. (2006) suggested that the overflow through the Luzon Strait has a notable impact on the circulation and water property distributions in the deep SCS. Through a set of sensitivity experiments using an ocean general circulation model, Lan et al. (2013) revealed that the Luzon overflow controls the formation of the deep cyclonic gyre in the SCS.

Based on *in-situ* observations, the Luzon overflow has two primary inlets (Fig. 1b). The northern inlet has an average volume transport of ~0.7×10^6 m^3/s, while the southern inlet has an average volume transport of ~0.9×10^6 m^3/s (Zhao et al., 2014). In addition, it has been shown that the transport across both inlets possesses significant intraseasonal variations in the 20–60 d band and seasonal variations in the 100–360 d band (Zhao et al., 2014; Zhou et al., 2014; Ye et al., 2019). To the best of our knowledge, the role that the overflows from two inlets play in driving the SCS deep circulation has not been studied. Furthermore, previous studies have shown that the deep SCS circulation also has a significant impact on the sediment transport over the northern

Foundation item: The Foundation of China Ocean Mineral Resources R&D Association under contract No. DY135-E2-2-02; the National Natural Science Foundation of China under contract Nos 91428206, 41976028 and 41806019.
*Corresponding author, E-mail: chencl@fudan.edu.cn

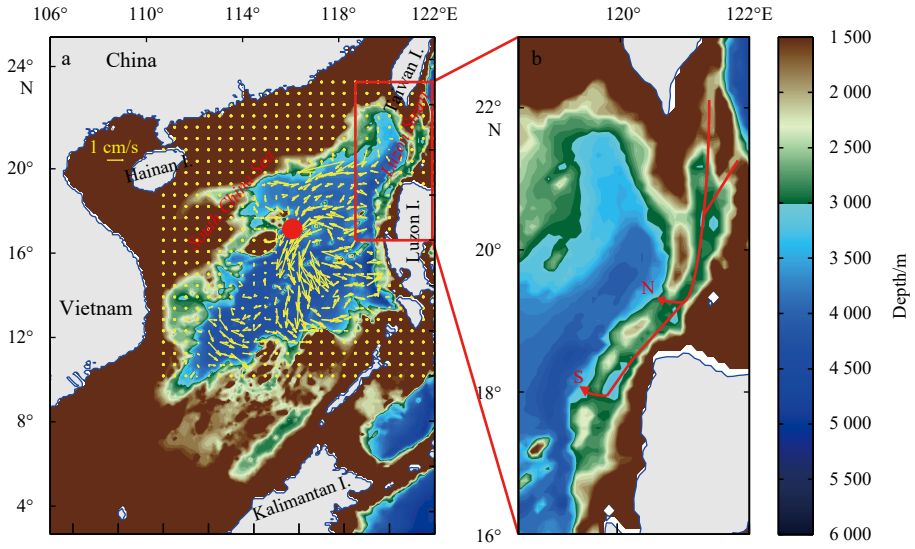

Fig. 1. Bottom topography (color shading) of the SCS and the vertically-averaged geostrophic current (vector) from 2 400 m to the bottom derived from U.S. Navy Generalized Digital Environment Model (GDEM) Version 3.0 (a), and bottom topography (color shading, m) and the schematic flow (red vector lines) across the Luzon Strait with N and S indicating the northern and southern inlets of the Luzon overflow (b). The red dot in a indicates the mooring location used in this study.

SCS (Shao et al., 2007; Zheng and Yan, 2012; Liu and Stattegger, 2014; Zhang et al., 2014). However, the effects of the two different inlets of the Luzon overflow on the sediment transport are also unknown.

This study begins by using an inverse reduced-gravity model to examine the influence of the Luzon overflow across the two deep inlets on the deep circulation in the SCS. The study then moves to the application of a Lagrangian trajectory model to study the possible effect that Luzon overflow across the two inlets may have on the sediment transport over the northern SCS. The paper is organized as follows: The data and inverse reduced-gravity model are introduced in Section 2. The applicability of the inverse reduced-gravity model to the circulation in deep SCS is evaluated in Section 3. The numerical results of the deep circulation in the northern SCS are described and analyzed in Section 4. Finally, discussion and summary are provided in Section 5.

2 Data and model

2.1 *Data*

To observe the deep current in the SCS, a current meter mooring, M1, was deployed in the deep western boundary zone of the SCS (16.6°N, 115.6°E; red dot in Fig. 1a) from June 2017 to September 2018. The water depth at the mooring location was 4 149 m and Recording Current Meters (RCMs) were mounted at 2 226 m, 3 226 m and 3 726 m to monitor the horizontal velocity of the deep flow.

The U.S. Navy GDEM V3.0 monthly climatology of observed temperature and salinity, with a horizontal resolution of 0.25° × 0.25°, was also used in this study. This data set has 78 standard depths from the surface down to 6 600 m, with a vertical resolution varying from 2 m at the surface to 200 m below 1 600 m (Carnes, 2009). The geostrophic velocity was calculated from the GDEM V3.0 using the thermal wind relation assuming the depth of no motion to be at 2 400 m. The idea of selecting a level of no motion has been used extensively in study of abyssal circulation (Stommel and Arons, 1959–1960a; Speer et al., 1993; Wang et al., 2011).

2.2 *Inverse reduced-gravity model*

For the circulation of deep basin, the flow near the bottom has been observed to be faster than that above it (Section 3.1). Therefore, an approximation can be made that the upper layer pressure gradient is negligible, so that we can set up an inverse reduced-gravity model on a β-plane:

$$\frac{\partial hu}{\partial t}+hu\frac{\partial u}{\partial x}+hv\frac{\partial u}{\partial y}+u\frac{\partial hu}{\partial x}+v\frac{\partial hu}{\partial y}-fhv = -g'h\frac{\partial \eta}{\partial x}+a_{\mathrm{h}}\left(\frac{\partial^2 hu}{\partial x^2}+\frac{\partial^2 hu}{\partial y^2}\right)-R\frac{hu}{h_0}, \tag{1a}$$

$$\frac{\partial hv}{\partial t}+hu\frac{\partial v}{\partial x}+hv\frac{\partial v}{\partial y}+u\frac{\partial hv}{\partial x}+v\frac{\partial hv}{\partial y}+fhu = -g'h\frac{\partial \eta}{\partial y}+a_{\mathrm{h}}\left(\frac{\partial^2 hv}{\partial x^2}+\frac{\partial^2 hv}{\partial y^2}\right)-R\frac{hv}{h_0}, \tag{1b}$$

$$\frac{\partial h}{\partial t}+\frac{\partial hu}{\partial x}+\frac{\partial hv}{\partial y}=-w, \tag{1c}$$

where x and y are zonal and meridional coordinates and u and v are the horizontal velocity components, respectively; f=βy is the Coriolis parameter; g'=0.03 is the reduced gravity; R/h_0, a_{h} are the parameters for the bottom friction and horizontal momentum dissipation, respectively, which are set to R = 10^{-3} m/s, a_{h} = 300 m^2/s. The thickness of the water column h is defined as:

$$h=h_0-h_{\mathrm{b}}-\eta, \tag{2}$$

where h_0 = 3 000 is the vertical thickness of the deep-water column; h_{b} is the prescribed bathymetry; and η is the deviation of the interface. The inverse reduced-gravity model has been widely used in deep ocean circulation studies (Stommel and Arons, 1959–1960a; Speer et al., 1993; Wang et al., 2018).

The model domain comprises the SCS central basin (9°–22°N, 111°–122°E). The resolution is (1/6)° ×(1/6)°. The deep SCS circu-

lation is forced by a uniform upwelling, w, and the deep Luzon overflow on a β-plane. The transport in the Luzon overflow has been estimated to be between 0.7×10^6–3.0×10^6 m^3/s based on different observations and model results (Wang, 1986; Liu and Liu, 1988; Qu et al., 2006; Tian et al., 2006; Zhao et al., 2014). In this study, based on *in-situ* observational results from Zhao et al. (2014) where we set the average Luzon overflow to be 1.6×10^6 m^3/s with 0.7×10^6 m^3/s entering through the northern inlet and 0.9×10^6 m^3/s entering through the southern inlet (CTRL case). The wall boundary condition was used except for the two inflows through the Taltung Canyon (0.4×10^6 m^3/s) and the Bashi Channel (1.2×10^6 m^3/s) in the model domain. In order to satisfy basin-wide mass conservation, a spatially uniform upwelling of 1×10^{-6} m/s is set, so that the total upwelling transport over the area of model domain matches the total transport of the deep Luzon overflow (1.6×10^6 m^3/s).

In order to investigate the influence of the Luzon overflow through the two inlets, we also consider two groups of experiments, one group has two cases where only 0.7×10^6 m^3/s (upwelling is 4.38×10^{-7} m/s to satisfy the mass conservation, inflows of Taltung Canyon and Bashi Channel are 0.175×10^6 m^3/s and 0.525×10^6 m^3/s) of the Luzon overflow occurs through the northern inlet (Case-N1) and only 0.9×10^6 m^3/s (upwelling is 5.62×10^{-7} m/s to satisfy the mass conservation, inflows of Taltung Canyon and Bashi Channel are 0.225×10^6 m^3/s and 0.675×10^6 m^3/s) of the Luzon overflow occurs through southern inlet (Case-S1), the other group has two cases where all 1.6×10^6 m^3/s of the Luzon overflow occurs through the northern (Case-N2) or southern (Case-S2) inlets. In all the cases, the transport ratio between the northern and southern inlets are controlled by adjusting the inlet topography. The simple model is spun-up for 10 years to reach a quasi-steady state, and then run for an additional 5 years, and the average result of the last 5 years is computed and analyzed. The details of these experimental cases are listed in Table 1.

Table 1. Details of the numerical experiment

Case	Overflow	Other settings
CTRL	1.6×10^6 m^3/s, 0.7×10^6 m^3/s from northern inlet and 0.7×10^6 m^3/s southern inlet	β-plain, uniform upwelling and with bottom topography
Case-N1	only 0.7×10^6 m^3/s, all from northern inlet	
Case-S1	only 0.9×10^6 m^3/s, all from southern inlet	
Case-N2	1.6×10^6 m^3/s, all from northern inlet	
Case-S2	1.6×10^6 m^3/s, all from southern inlet	

2.3 *TRACMASS—a Lagrangian trajectory model*

The Lagrangian trajectory model, TRACMASS (Döös et al., 2013) was used on the inverse reduced-gravity model results to calculate the particle trajectories. The theory behind the original scheme for steady state velocities was derived for rectangular and curvilinear grids using different vertical coordinates for the oceanic and atmospheric circulation models. The TRACMASS trajectories are exact solutions to differential equations and can therefore be integrated both forward and backward with unique solutions. The TRACMASS has been effectively used for the deep meridional overturning circulation (MOC) in the SCS (Shu et al., 2014). In this study, we only use the horizontal velocities in the TRACMASS as the inverse reduced-gravity model has no vertical velocity component.

3 The applicability of the inverse reduced-gravity model for the deep SCS circulation

3.1 *The bottom intensification in the deep SCS*

Figure 1a shows the vertical-averaged geostrophic current (cm/s) from 2 400 m to bottom in the deep SCS derived from GDEM. There is a significant cyclonic circulation with an obvious DWBC. The velocity of the DWBC is O(1 cm/s) with maximum values located around 16°N. In order to visualize the vertical distribution of the current, a vertical cross-section of the current speed at 18°N is shown in Fig. 2. It shows that the geostrophic current speed increases from 0 at 2 400 m (depth of no motion) to a maximum of 1.2 cm/s at the bottom.

To verify this vertical structure of the DWBC in the SCS, we analyzed the *in-situ* data from the M1 mooring. All observed current time-series were 72-h low-pass filtered to remove the inertial and major tidal signals (Godin, 1966). The average velocity components (u, v) at 2 226 m, 3 226 m and 3 726 m were (–0.94 cm/s, –0.56 cm/s), (–2.69 cm/s, –0.57 cm/s) and (–3.36 cm/s, –0.58 cm/s), respectively, showing a remarkable deep southwestward flow (Fig. 3a). The time averaged current speed for the three current meter depths in the deep SCS were 1.10 cm/s, 2.74 cm/s and 3.41 cm/s, respectively (Fig. 3b). This is consistent with the GDEM results suggesting that the flow speeds increase with depth. Both the GDEM results and *in-situ* observations verify the bottom intensification of the deep circulation in the deep SCS (Figs 2 and 3b), which suggests that the inverse reduced-gravity model can be used to simulate the deep SCS circulation.

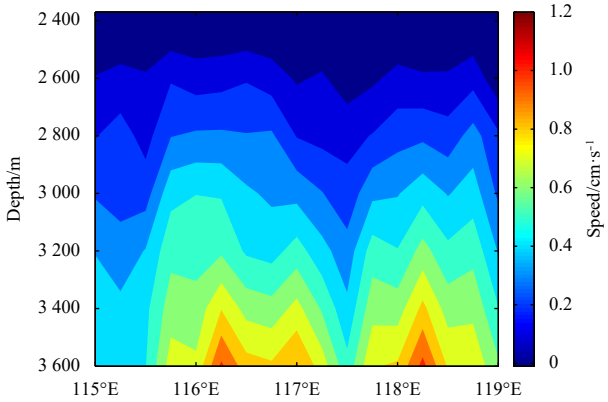

Fig. 2. Geostrophic current speed below 2 400 m at 18°N in the SCS calculated from GDEM assuming a depth of no motion at 2 400 m.

3.2 *The utility of the model in the deep SCS*

The inverse reduced-gravity model was formulated to investigate the influence of the Luzon overflow on the deep circulation in the SCS. We begin by considering the control case (CTRL) with the total Luzon overflow transport of 1.6×10^6 m^3/s, value taken from the observations of Zhao et al. (2014) and listed in Table 1.

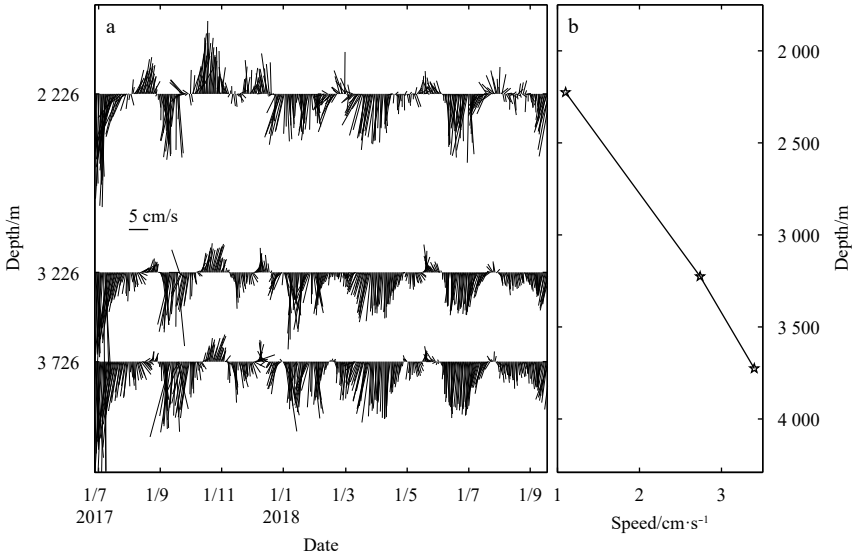

Fig. 3. Horizontal velocity time series (a) and its temporal average (b) at M1 mooring.

The experimental result shows that the abyssal circulation in the SCS is cyclonic with strong DWBC (CTRL, Fig. 4). Generally, this deep circulation pattern seen in the CTRL case is consistent with that from the GDEM result (Fig. 1a).

We further compare the mean current speed between 17.5°–19.5°N along meridional section and the mean current speed between 114°–116°E along the zonal section from our model results to the GDEM results (Fig. 5). Although the currents in the model are generally stronger than those estimated from the GDEM results, possibly due to the smoothing/averaging process in the GDEM, they show similar variations. For example, the maximum flows located at 117°E along the northern boundary and at 16.5°N along the western boundary are quite similar. In addition, the time averaged current speed from the M1 mooring location at 16.6°N/115.6°E was about 2 cm/s, which matches the reduced-gravity model results.

All these results suggest that, despite some differences in magnitude, the relatively simple reverse reduced-gravity model can capture the general features of the deep circulation and the

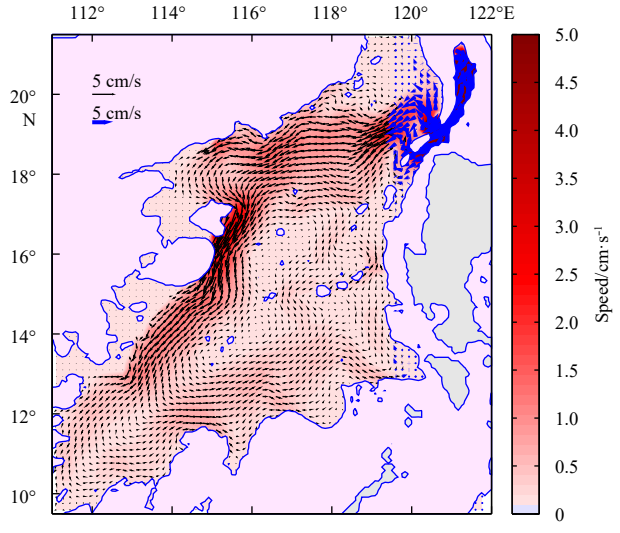

Fig. 4. The abyssal circulation (vectors) and current speed (color shading) for the control case (CTRL).

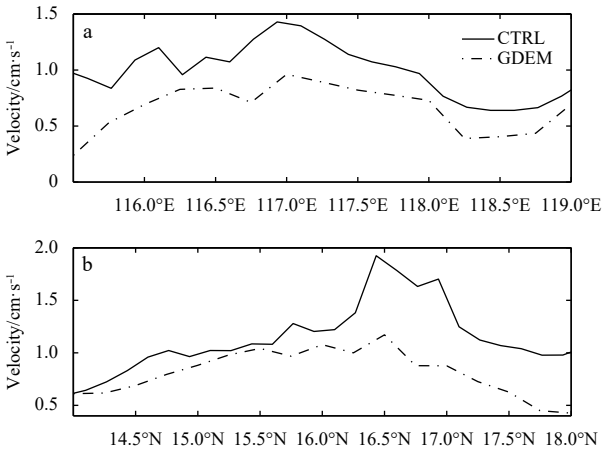

Fig. 5. The mean current speed between 17.5°–19.5°N along meridional section (a) and the mean current speed between 114°–116°E along the zonal section (b) from the CTRL case (black lines) and GDEM (black dashed lines).

DWBC in the SCS seen in both the GDEM results and *in-situ* observations. These differences in magnitude are likely from the model performances. However, the similarity between the CTRL experiment and GDEM result provides confidence that the reduced-gravity model can be applied to further explore the effects of Luzon overflow through the northern and southern inlets.

4 Influence of the Luzon overflow inlets on the deep northern SCS circulation

To investigate the separate effects of overflow through the northern and southern inlets on the deep circulation in the SCS, Case-N1 (observed overflow with 0.7×10^6 m^3/s in the northern inlet only) and Case-S1 (observed overflow with 0.9×10^6 m^3/s in the southern inlet only) are conducted. Figures 6a and b show the abyssal circulation in these two experiments. As expected, because of lower overflow input, the dominant features in both cases are a cyclonic deep circulation whose intensity is weaker than that in the CTRL. It is worth noting that the difference

between the CTRL experiment and the sum of the Case-N1 and Case-S1 experiments is small (Fig. 6c), indicating that the response of the deep circulation to northern and southern inlet overflows is nearly linear. We quantify the contributions of the two inlets to the deep SCS circulation by calculating the average speed between 17.5°–19.5°N along meridional section (Fig. 6d). These result show that the northern (southern) inlet accounts for about 46% (54%) of the deep circulation in the SCS, broadly in line with the relative overflow contributions from the two inlets (44% in the northern inlet and 56% in the northern inlet). However, a recent study from Ye et al. (2019) showed that the overflow through the northern inlet may actually be larger than that through the southern inlet, opposite to the result of Zhao et al. (2014). Therefore, until the relative contribution of each inlet to the total mass flow through the Luzon Strait is definitively determined, the question as to which inlet is more important to the deep circulation in the SCS cannot be answered.

Based on the above results, we find that the relative contribution of the Luzon overflow in the northern (southern) inlet is not exactly equal to its contribution to the deep SCS circulation, which implies that it is not clear that which inlet is more efficient in driving deep SCS circulation. Therefore, two experiments with identical overflows input through either the northern inlet (Case-N2) or the southern inlet (Case-S2) are conducted to address this issue. Figure 7 shows the abyssal circulation anomalies relative to the CTRL for these two experiments. The most notable feature in these results is that the influence of the overflows is largely restricted to the northern SCS. In addition, when the overflow is confined to the northern inlet (Case-N2), there is an anomalous cyclonic circulation in the basin north of 17°N with a prominent southwestward current exceeding 2 cm/s at the northern boundary (Fig. 7a). Conversely, when the overflow is confined to the southern inlet (Case-S2), an anti-cyclonic circulation anomaly appears in the northern SCS with an obvious northeastward current at the northern boundary (Fig. 7b). When the mean speed between 17.5°–19.5°N along meridional section from these two cases and CTRL are compared (Fig. 8a), it is clear that the deep current in the northern SCS is enhanced when the overflow enters through the northern inlet and weakened when it enters through the southern inlet. Consequently, the overflow through the northern inlet is more efficient than the southern inlet in driving the deep circulation in the northern SCS. To be more specific, the mean speed in the northern SCS is about 1.21 cm/s in the CTRL, 1.26 cm/s in the Case-N2, and 1.17 cm/s in the Case-S2. The anomalous circulation in the northern part of the SCS may be explained through source-sink theory from Stommel et al. (1958). The schematic source-sink diagrams, in which zonal geostrophic flow extends from the source to the western bound-

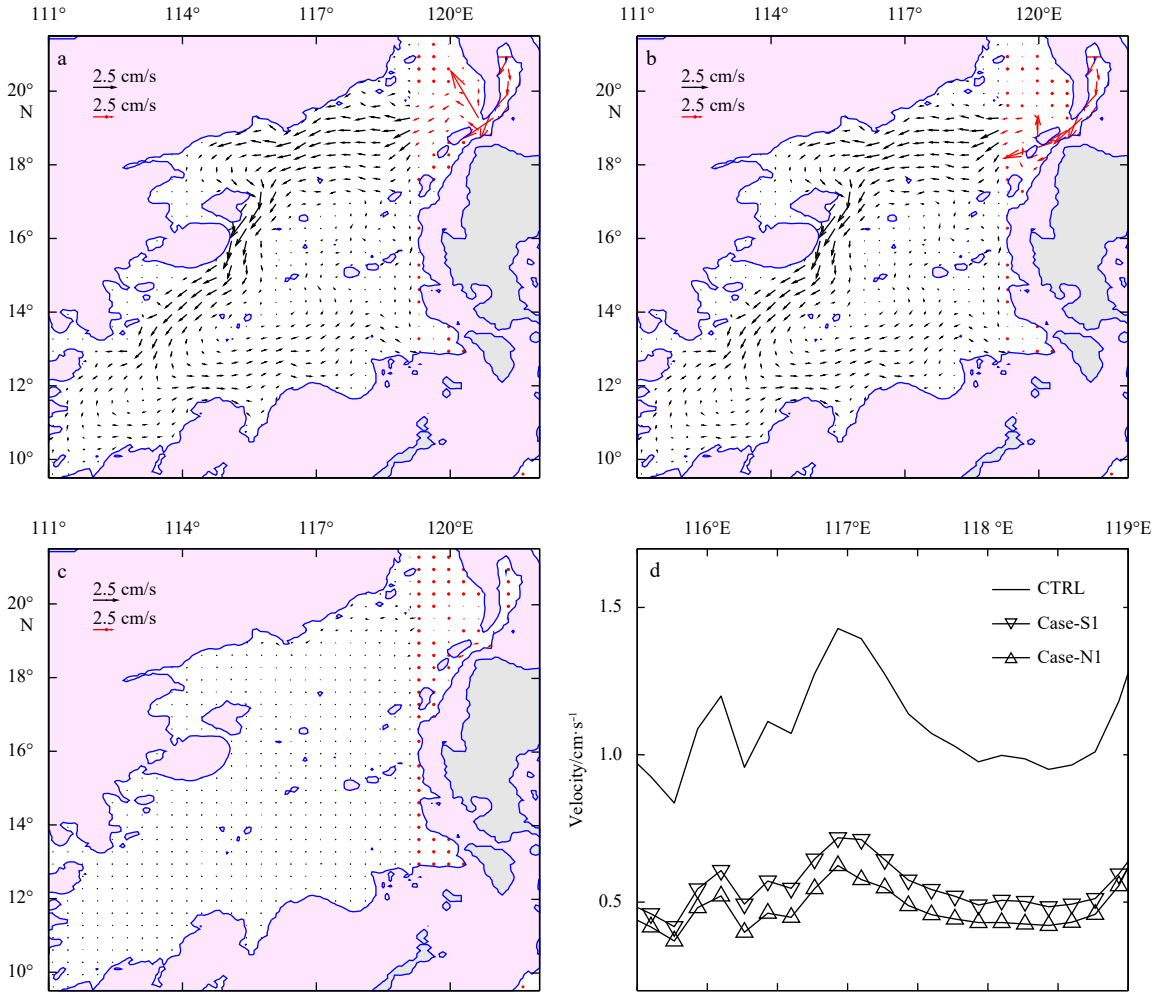

Fig. 6. The abyssal circulation from Case-N1 (a) and Case-S1 (b), the abyssal circulation anomalies for Case-N1 plus Case-S1 minus CTRL (c), and the mean current speed between 17.5°–19.5°N along meridional section from the CTRL (black solid line), Case-N1 (black solid line with northward triangle), and Case-S1 (black solid line with southward triangle) (d).

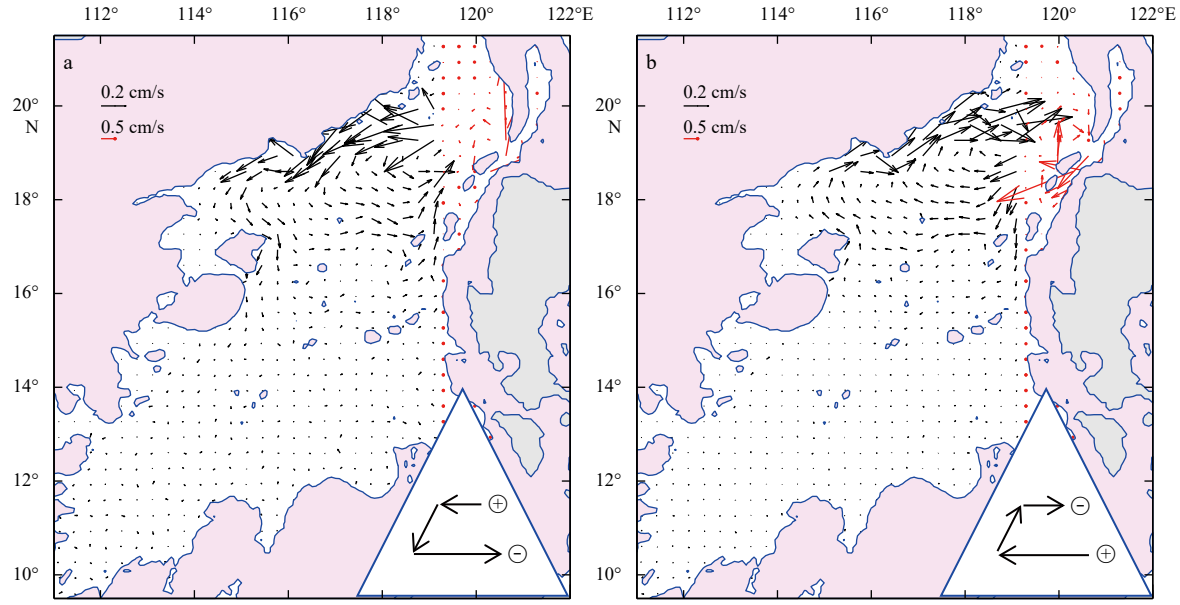

Fig. 7. The abyssal circulation anomalies for Case-N2 (a) and Case-S2 (b). The schematic diagram at the lower right indicates the general source-sink circulation pattern. Compared to the CTRL, the forcing in the Case-N2 is a 0.9×10^6 m^3/s source at the northern inlet and a 0.9×10^6 m^3/s sink at the southern inlet; while for the Case-S2, there is a 0.7×10^6 m^3/s sink at the northern inlet and a 0.7×10^6 m^3/s source at the southern inlet.

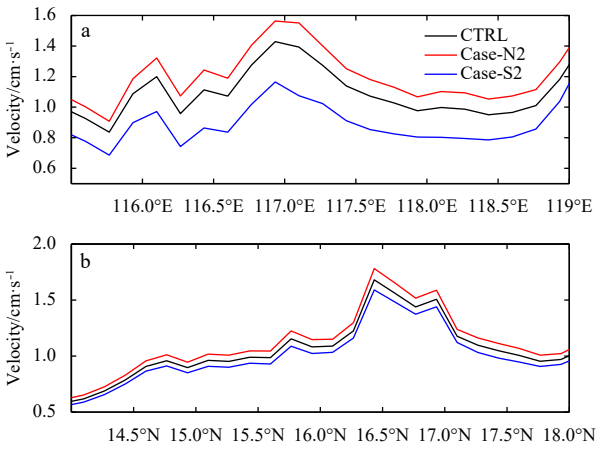

Fig. 8. The mean current speed between 17.5°–19.5°N along meridional section (a) and the mean current speed between 114°–116°E along the zonal section (b) from the CTRL case (black lines), Case-N2 (red line), and Case-S2 (blue line).

ary, then flows along the western boundary in a narrow zone, and then flows eastward to the sink are included at the bottom right of each panel in Fig. 7.

In addition to the source-sink theory, the difference in the response of the deep circulation to overflow through the two inlets can be partially explained by PV conservation theory. The PV conservation dictates that the SCS basin integrated PV integral yields a balance between the net lateral PV inflow and the internal PV dissipation by Rayleigh friction (Lan et al., 2013). According to Yang and Price (2000), the balance can be written as:

$$f\frac{Q_{\mathrm{Luzon}}}{H_{\mathrm{Luzon}}} = -\lambda \oint (\boldsymbol{u}\cdot\boldsymbol{l})\,\mathrm{d}l, \tag{3}$$

where f is the Coriolis parameter, Q_{Luzon} is the volume transport and H_{Luzon} is the layer thickness of the deep overflow through the Luzon Strait, λ is the Rayleigh friction coefficient, $\boldsymbol{u}$ is the basin-scale SCS deep circulation, and $\boldsymbol{l}$ is the coordinate parallel to the boundary. When there is positive PV transport into the deep SCS, the deep circulation becomes more cyclonic to satisfy the integral balance. The PV balance dictates that the stronger (weaker) PV inflow enhances (weakens) the cyclonic circulation. In the Luzon Strait, the PV inflow of the two inlets is $f_{\mathrm{N}}(Q_{\mathrm{N}}/H_{\mathrm{N}}) + f_{\mathrm{S}}(Q_{\mathrm{S}}/H_{\mathrm{S}})$ (where f_{N}=$f_{19\mathrm{N}}$, f_{S}=$f_{18\mathrm{N}}$, Q_{N}=0.7×10^6 m^3/s, Q_{S}=0.9×10^6 m^3/s, H_{N}=320 m, H_{S}=560 m). When the entire Luzon overflow enters through the northern inlet (Q_{N}=1.6×10^6 m^3/s, Q_{S}=0.0 m^3/s), there is increased PV inflow and the cyclonic circulation is enhanced to balance this positive PV input. The situation is reversed when the entire Luzon overflow enters through the southern inlet. These results are consistent with the PV constraint theory of Yang and Price (2000) and Yang (2005).

In general, both source-sink theory and PV constraint theory can be used to explain the deep circulation anomaly in the northern SCS, the PV constraint theory can further explain why the intensification of the deep circulation is not only confined to the northern SCS, but also occurs in the southern SCS (Fig. 8b) in the Case-N2.

While the above discussion uncovers the differences in the deep SCS circulation as a result of changing the inlet of the Luzon overflow, it is of interest to consider how these changes might impact the sediment transport over the northern SCS (Shao et al., 2007; Zheng and Yan, 2012; Zhang et al., 2014). Using the TRACMASS system, we introduce five tracer parcels in the Luzon trough outlet, upstream of the two inlets, to study the effect of changing the location of inlet in the Luzon overflow on sedimentary processes. The trajectories of the tracers after 30 d in the CTRL, Case-N2 and Case-S2 are shown in Fig. 9. In the CTRL (Fig. 9a), two parcels (40%) entered the SCS through the northern inlet, while the other three (60%) entered the SCS through the southern inlet. The trajectories are basically along the currents,

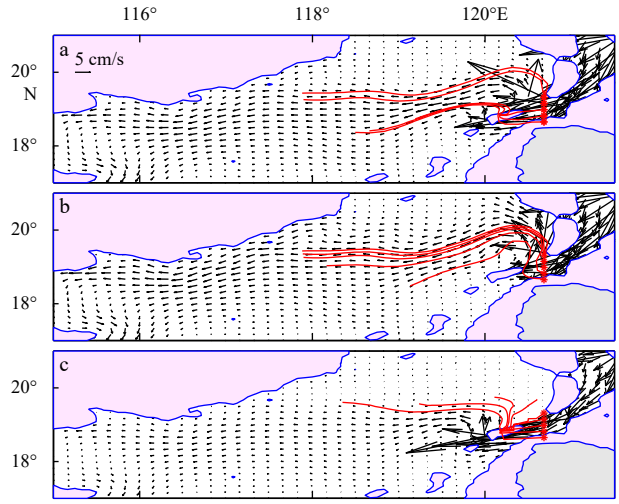

Fig. 9. The trajectories of five tracer parcels in the CTRL (a), Case-N2 (b) and Case-S2 (c). The black arrows denote the abyssal circulation.

this means that if there are sediments in the deep Luzon Strait, they will enter into the SCS along the currents, and the deep circulation in the SCS will affect the deposition and transport process.

Because the Luzon overflow in Case-N2 (Case-S2) enters entirely through the northern (southern) inlet, all of the tracer parcels enter the SCS through that inlet (Figs 9b and c). Since the deep circulation gyre is enhanced (weakened) when all of the Luzon overflow water enters the SCS through the northern (southern) inlet, the tracers flow more quickly (slowly) and follow a more northward (southward) path than in the CTRL. The implication of these results may provide some insight into the research on sediment transport processes in the deep SCS.

5 Discussion and summary

The circulation in the deep SCS, including the DWBC, are primarily forced by the Luzon overflow (Qu et al., 2006; Wang et al., 2011; Lan et al., 2013) through two inlets (Zhao et al., 2014; Ye et al., 2019). In this study, we have considered these two inlet overflows in isolation to investigate the influence of the Luzon overflow through the two inlets on the deep circulation in the northern SCS. It is suggested that the relative contribution of the two inlets is mainly relied on the input transport of the overflow, but overflow through the northern inlet is more efficient in driving the deep circulation in the northern SCS than through the southern inlet. When the Luzon overflow enters into the SCS entirely through the northern (southern) inlet, the deep cyclonic circulation in the northern SCS is enhanced (weakened). The results from a Lagrangian analysis suggests that different Luzon overflow location may also impact on the sediment transport over the northern SCS.

As previously mentioned, the observed transport of Luzon overflow, including the overflow through the northern and southern inlets, has obvious intraseasonal and seasonal variations (Zhao et al., 2014; Zhou et al., 2014; Zhang et al., 2015; Ye et al., 2019). However, while some inferences from this study could be made, the effects of these seasonal and intraseasonal variabilities of Luzon overflow on the deep SCS circulation have not been studied clearly and are worth further investigation.

In this study, as in previous abyssal circulation studies (Stommel and Arons, 1959–1960b; Speer et al., 1993), a uniform upwelling was assumed to balance the mass inputs from the Luzon overflow. However, recent observations have shown that diapycnal mixing rates in the deep ocean are several orders of magnitude larger near steep bathymetry (e.g., Kunze and Sanford, 1996; Ledwell et al., 2000; Mauritzen et al., 2002; Heywood et al., 2002; St Laurent and Garrett, 2002; Garabato et al., 2004), indicating that significant spatial variations likely exist in the upwelling. Recently, Wang et al. (2018) revealed that different upwelling/downwelling pattern has a significant impact on the deep SCS circulation by the numerical modelling. Therefore, more realistic upwelling patterns needs to be observed and the impacts of these spatial variations on the deep SCS circulation need to be studied.

Further, the reverse reduced-gravity model is employed herein because it is still very difficult to simulate the deep SCS circulation using high-resolution three-dimensional ocean general circulation models (OGCM) due to a weak understanding of the full complexity of the deep SCS system (Tian and Qu, 2012). More comprehensive diagnosis and analysis of the dynamics of the deep circulation in the SCS requires both the development of better OGCM simulation skills and improved *in-situ* observations in the future.

Acknowledgements

The topography data is available at http://ngdc.noaa.gov/mgg/global/global.hmtl. The GDEM Version 3.0 is available at https://esme.bu.edu/download. We thank the mooring group for their support in the mooring operation.

References

Carnes M R. 2009. Description and Evaluation of GDEM-V3.0. Naval Research Laboratory (NRL) Report NRL/MR/7330-09-9165. Washington, DC: Naval Research Laboratory

Chang Y T, Hsu W L, Tai J H, et al. 2010. Cold deep water in the South China Sea. Journal of Oceanography, 66(2): 183–190, doi: 10.1007/s10872-010-0016-x

Döös K, Kjellsson J, Jönsson B. 2013. TRACMASS—A Lagrangian trajectory model. In: Soomere T, Quak E, eds. Preventive Methods for Coastal Protection. Heidelberg: Springer, 225–249

Garabato A C N, Polzin K L, King B A, et al. 2004. Widespread intense turbulent mixing in the southern ocean. Science, 303(5655): 210–213, doi: 10.1126/science.1090929

Godin G. 1966. Daily mean sea level and short-period seiches. International Hydrographic Review, 43(2): 75–89

Heywood K J, Garabato A C, Stevens D P. 2002. High mixing rates in the abyssal Southern Ocean. Nature, 415(6875): 1011–1014, doi: 10.1038/4151011a

Kunze E, Sanford T B. 1996. Abyssal mixing: Where it is not. Journal of Physical Oceanography, 26(10): 2286–2296, doi: 10.1175/1520-0485(1996)026<2286:AMWIIN>2.0.CO;2

Lan Jian, Wang Yu, Cui Fengjuan, et al. 2015. Seasonal variation in the South China Sea deep circulation. Journal of Geophysical Research: Oceans, 120(3): 1682–1690, doi: 10.1002/2014JC010413

Lan Jian, Zhang Ningning, Wang Yu. 2013. On the dynamics of the South China Sea deep circulation. Journal of Geophysical Research: Oceans, 118(3): 1206–1210, doi: 10.1002/jgrc.20104

Ledwell J R, Montgomery E T, Polzin K L, et al. 2000. Evidence for enhanced mixing over rough topography in the abyssal ocean. Nature, 403(6766): 179–182, doi: 10.1038/35003164

Li Li, Qu Tangdong. 2006. Thermohaline circulation in the deep South China Sea basin inferred from oxygen distributions. Journal of Geophysical Research, 111: C05017

Liu C T, Liu R J. 1988. The deep current in the Bashi Channel. Acta Oceanographica Taiwanica, 20: 107–116

Liu Zhifei, Stattegger K. 2014. South China Sea fluvial sediments: An introduction. Journal of Asian Earth Sciences, 79: 507–508, doi: 10.1016/j.jseaes.2013.11.003

Mauritzen C, Polzin K L, McCartney M S, et al. 2002. Evidence in hy-

drography and density fine structure for enhanced vertical mixing over the Mid-Atlantic Ridge in the western Atlantic. Journal of Geophysical Research, 107(C10): 3147, doi: 10.1029/2001JC001114

Qu Tangdong. 2002. Evidence for water exchange between the South China Sea and the Pacific Ocean through the Luzon Strait. Acta Oceanologica Sinica, 21(2): 175–185

Qu Tangdong, Girton J B, Whitehead J A. 2006. Deepwater overflow through Luzon Strait. Journal of Geophysical Research: Oceans, 111: C01002

Shao Lei, Li Xuejie, Geng Jianhua, et al. 2007. Deep water bottom current deposition in the northern South China Sea. Science in China Series D: Earth Sciences, 50(7): 1060–1066, doi: 10.1007/s11430-007-0015-y

Shu Yeqiang, Xue Huijie, Wang Dongxiao, et al. 2014. Meridional overturning circulation in the South China Sea envisioned from the high-resolution global reanalysis data GLBa0.08. Journal of Geophysical Research: Oceans, 119(5): 3012–3028, doi: 10.1002/2013JC009583

Shu Yeqiang, Xue Huijie, Wang Dongxiao, et al. 2016. Persistent and energetic bottom-trapped topographic Rossby waves observed in the southern South China Sea. Scientific Reports, 6: 24338, doi: 10.1038/srep24338

Speer K, Tziperman E, Feliks Y. 1993. Topography and grounding in a simple bottom layer model. Journal of Geophysical Research, 98(C5): 8547–8558, doi: 10.1029/92JC03018

St Laurent L, Garrett C. 2002. The role of internal tides in mixing the deep ocean. Journal of Physical Oceanography, 32(10): 2882–2899, doi: 10.1175/1520-0485(2002)032<2882:TROITI>2.0.CO;2

Stommel H, Arons A B. 1959–1960a. On the abyssal circulation of the World Ocean-I. Stationary planetary flow patterns on a sphere. Deep Sea Research, 6: 140–154, doi: 10.1016/0146-6313(59)90065-6

Stommel H, Arons A B. 1959–1960b. On the abyssal circulation of the World Ocean-II. An idealized model of the circulation pattern and amplitude in oceanic basins. Deep Sea Research, 6: 217–233, doi: 10.1016/0146-6313(59)90075-9

Stommel H, Arons A B, Faller A J. 1958. Some examples of stationary planetary flow patterns in bounded basins. Tellus, 10(2): 179–187, doi: 10.3402/tellusa.v10i2.9238

Tian Jiwei, Qu Tangdong. 2012. Advances in research on the deep South China Sea circulation. Chinese Science Bulletin, 57(24): 3115–3120, doi: 10.1007/s11434-012-5269-x

Tian Jiwei, Yang Qiangxuan, Liang Xinfeng, et al. 2006. Observation of Luzon Strait transport. Geophysical Research Letters, 33(19): L19607, doi: 10.1029/2006GL026272

Tian Jiwei, Yang Qingxuan, Zhao Wei. 2009. Enhanced Diapycnal Mixing in the South China Sea. Journal of Physical Oceanography, 39(12): 3191, doi: 10.1175/2009JPO3899.1

Wang Aimei, Du Yan, Peng Shiqiu, et al. 2018. Deep water characteristics and circulation in the South China Sea. Deep Sea Research Part I: Oceanographic Research Papers, 134: 55–63, doi: 10.1016/j.dsr.2018.02.003

Wang Dongxiao, Wang Qiang, Cai Shuqun, et al. 2019. Advances in research of the mid-deep South China Sea circulation. Science China Earth Sciences, 62(12): 1992–2004, doi: 10.1007/s11430-019-9546-3

Wang Dongxiao, Xiao Jingen, Shu Yeqiang, et al. 2016. Progress on deep circulation and meridional overturning circulation in the South China Sea. Science China Earth Sciences, 59(9): 1827–1833, doi: 10.1007/s11430-016-5324-6

Wang Guihua, Xie Shangping, Qu Tangdong, et al. 2011. Deep South China Sea circulation. Geophysical Research Letters, 38(5): L05601

Wang J. 1986. Observation of abyssal flows in the northern South China Sea. Acta Oceanographica Taiwanica, 16: 36–45

Wyrtki K. 1961. Physical oceanography of the Southeast Asian waters. In: NAGA Report Volume 2, Scientific Results of Marine Investigations of the South China Sea and the Gulf of Thailand. San Diego, California: Scripps Institution of Oceanography

Yang Jiayan. 2005. The arctic and subarctic ocean flux of potential vorticity and the arctic ocean circulation. Journal of Physical Oceanography, 35(12): 2387–2407, doi: 10.1175/JPO2819.1

Yang Jiayan, Price J F. 2000. Water-mass formation and potential vorticity balance in an abyssal ocean circulation. Journal of Marine Research, 58(5): 789–808, doi: 10.1357/002224000321358918

Yang Qingxuan, Zhao Wei, Liang Xinfeng, et al. 2016. Three-dimensional distribution of turbulent mixing in the South China Sea. Journal of Physical Oceanography, 46(3): 769–788, doi: 10.1175/JPO-D-14-0220.1

Ye Ruijie, Zhou Chun, Zhao Wei, et al. 2019. Variability in the deep overflow through the Heng-Chun Ridge of the Luzon Strait. Journal of Physical Oceanography, 49(3): 811–825, doi: 10.1175/JPO-D-18-0113.1

Zhang Yanwei, Liu Zhifei, Zhao Yulong, et al. 2014. Mesoscale eddies transport deep-sea sediments. Scientific Reports, 4(1): 5937

Zhang Zhiwei, Zhao Wei, Tian Jiwei, et al. 2015. Spatial structure and temporal variability of the zonal flow in the Luzon Strait. Journal of Geophysical Research: Oceans, 120(2): 759–776, doi: 10.1002/2014JC010308

Zhao Wei, Zhou Chun, Tian Jiwei, et al. 2014. Deep water circulation in the Luzon Strait. Journal of Geophysical Research: Oceans, 119(2): 790–804, doi: 10.1002/2013JC009587

Zheng Hongbo, Yan Pin. 2012. Deep-water bottom current research in the Northern South China Sea. Marine Georesources and Geotechnology, 30(2): 122–129, doi: 10.1080/1064119X.2011.586015

Zhou Chun, Zhao Wei, Tian Jiwei, et al. 2014. Variability of the deep-water overflow in the Luzon Strait. Journal of Physical Oceanography, 44(11): 2972–2986, doi: 10.1175/JPO-D-14-0113.1

Zhou Chun, Zhao Wei, Tian Jiwei, et al. 2017. Deep western boundary current in the South China Sea. Scientific Reports, 7(1): 9303, doi: 10.1038/s41598-017-09436-2